Carbon 134 (2018) 326–333

Contents lists available at ScienceDirect

Carbon

journal homepage: www.elsevier.com/locate/carbon

Thiolated-graphene-based supercapacitors with high energy density and stable cycling performance

Santhakumar Kannappan [a], Hao Yang [b], Karthikeyan Kaliyappan [c, e], Rajesh Kumar Manian [d], Amaresh Samuthira Pandian [e, f], Yun Sung Lee [e], Jae-Hyung Jang [a], Wu Lu [a, b, *]

[a] Department of Nanobio Materials and Electronics, Gwangju Institute of Science and Technology, Gwangju 500-712, Republic of Korea
[b] Department of Electrical and Computer Engineering, The Ohio State University, Columbus, OH 43210, USA
[c] Department of Mechanical and Materials Engineering, The University of Western Ontario, London, Ontario, N6A 5B9, Canada
[d] Biomolecular Sciences Institute, Department of Chemistry and Biochemistry, Florida International University, Miami, FL 33199, USA
[e] Faculty of Applied Chemical Engineering, Chonnam National University, Gwangju, 500-757, Republic of Korea
[f] Center for Nanophase Material Science, Oak Ridge National Laboratory, Oak Ridge, TN 37830, USA

ARTICLE INFO

Article history:
Received 23 June 2017
Received in revised form
29 January 2018
Accepted 7 February 2018
Available online 23 February 2018

ABSTRACT

We report supercapacitors based on thiolated-graphene (T-graphene) with stable charging and discharging performance at high current density. The T-graphene was synthesized using low cost NaSH as a reducing agent to reduce graphene oxide. X-ray diffraction (XRD) and x-ray photoelectron spectroscopy (XPS) studies reveal that NaSH is an effective reducing agent in removing oxygen containing groups from graphene oxide. The highly reduced T-graphene with a C/O ratio of 28 was used as the supercapacitor electrode material. At a current density of 2.5 Ag^{-1}, the T-graphene supercapacitor exhibited an electrochemical capacitance of 195 Fg^{-1}, a power density of 4.3 $kWkg^{-1}$and an energy density of 83.4 $Whkg^{-1}$. The time required to discharge 83.4$Whkg^{-1}$ at 2.5 Ag^{-1} is around 69 s. At a current density of 7.5 Ag^{-1}, the cell exhibited a specific capacitance of about 137 Fg^{-1} and retained 98% of its initial capacitance value after 10,000 cycles. This superior performance of supercapacitor can be ascribed to highly reduced and porous T-graphene with minimum restacking due to its crumpled nature. The resulting supercapacitors having stable performance at high current density are suitable for fast charging-discharging applications.

1. Introduction

Supercapacitors are very promising candidates for future energy storage technology [1,2]. Since there is no chemical reaction involved during charge storage in a supercapacitor based on electrochemical double-layer capacitance, stable operation exceeding one hundred thousand cycles is expected [2]. Commercial supercapacitors, which are based on activated carbon (AC), have achieved energy density in the range of 4–6 Wh/kg [3,4]. Considering that the energy densities of the conventional batteries such as lead-acid batteries, nickel-metal hydride batteries, lithium ion batteries are 30–40 Wh/kg [5–7], 60–80 Wh/kg [6,8], 100–275 Wh/kg [9], respectively, supercapacitors still need significant improvement in terms of energy density while maintaining their operational stability. Thus, it is critical to improve the energy density of supercapacitor to match energy density of conventional batteries without sacrificing the high power density and cycle life. Supercapacitors based on conducting polymers, especially polyaniline, can offer very high specific capacitance but exhibit poor cycling stability [10]. To improve the energy density of supercapacitors, carbon nanotube (CNT) based electrode materials [11,12] have been tested. However such materials lack of porous structures so the active area for charge storage is limited. To have high stability, recently graphene-based materials have been extensively studied because graphene is suitable for an active material in supercapacitors due to its large surface area and high electrical conductivity [13–17]. Liu et al. reported a graphene-based supercapacitor with high energy density of 88.2 Wh kg^{-1} [18].

* Corresponding author. Department of Electrical and Computer Engineering, The Ohio State University, Columbus, OH 43210, USA.
E-mail address: lu.173@osu.edu (W. Lu).

https://doi.org/10.1016/j.carbon.2018.02.036
0008-6223/

This was achieved due to the high surface area graphene with a curved morphology. Metal oxides, such as MgO, Fe_3O_4, MnO_2, and Co_3O_4, have been utilized in metal oxide graphene composites for the further specific capacitance performance improvement of supercapacitors [19–23]. Although these metal oxide graphene composites have improved the specific capacitance and energy density, the charging time and discharging time are too long for high-power applications. Degradation of specific capacitance due to Faradic reactions has also been observed in supercapacitors employing metal oxide graphene composites [16–18]. There have also been attempts to improve the electrochemical performance by using ionic liquids. Among them, 1-Ethyl-3-methylimidazolium tetrafluoroborate ($EMIMBF_4$) has a high conductivity as well as a wide potential window of 4 V, which are beneficial for specific capacitance improvement [15,18]. Yanwu et al. investigated the capacitance properties of graphene supercapacitors with ionic liquid, which yielded high energy density of 70 $Whkg^{-1}$ [15]. Further research in this area could lead to graphene-based supercapacitors with improved energy density that would be comparable with lithium ion batteries but with a higher power density, a rapid charging time and stable cycling performance.

A graphene supercapacitor stores charges on the porous surface of electrodes through physisorption of electrolyte ions. Therefore, it is critical to control exfoliation, morphology, and pore size distribution to achieve few-layered or even single-layer graphene nanosheets with larger surface area and higher ion accessibility [24]. There are several methods to synthesize graphene, such as chemical methods [25–27], sonication methods [28,29], microwave methods [18,30], electrochemical methods [31] and thermal methods [32]. In chemical methods, several reducing agents, such as hydrazine [33], NaOH [34], NaBH [35] and hydroquinone [36], have been used for reduction of graphene oxide (GO) in various media. These reducing agents are toxic and are difficult to handle during reduction, which is a disadvantage for large-volume production. For electrochemical energy storage applications, another issue these methods face is that during the reduction of GO to reduced graphene oxide (r-GO), graphene sheets are often stacking together due to van der Waals force, which may reduce the active surface area of the graphene. There has been growing demand for a cost effective, safe, and environmentally-friendly method to produce high-quality graphene nanosheets for energy storage.

Recently, it has been reported that thiolated graphene (T-graphene) exhibits catalytic activity and long-term durability [38]. Moreover, T-graphene has an advantage of not stacking together, which may allow electrolytes to access more pores. By functionalizing r-GO with thiol group, the restacking problem can be minimized. In this work, we present for the first time the fabrication of supercapacitors based on synthesized T-graphene as electrode materials. We synthesized T-graphene by a modified Hummer's method using NaSH as reducing agent [37,38]. This method prohibits the restacking or agglomeration of graphene layers after reduction and allows easier access to the graphene surface by electrolytes. A specific capacitance of 196 Fg^{-1}as well as an energy density of 83.36 $Whkg^{-1}$ were achieved at a current density of 2.5 Ag^{-1} at room temperature in a symmetrical supercapacitor. At high current density of 7.5 Ag^{-1}, the cell was found to be stable in terms of specific capacitance (137 Fg^{-1}) and energy density (58.25 $Whkg^{-1}$) after 10,000 cycles of operation.

2. Methodology

2.1. Preparation of graphite oxide

The modified Hummers method was utilized to prepare GO from graphite powder [38]. In brief, the graphite powder (4 g) was first pre-oxidized with a solution of H_2SO_4 (60 mL), $K_2S_2O_8$ (2 g), and P_2O_5 (2 g) at 80 °C. The resulting mixture, after cooling to room temperature, was filtered and washed until the rinse water became neutral. The oxidized graphite powder (2 g) was placed in concentrated H_2SO_4 (40 mL), and $KMnO_4$ (6 g) was added subsequently under stirring in an ice-bath. The mixture was then stirred for 2 h, further DI water (92 mL) was added. Next, additional DI water (280 mL) and 30% H_2O_2 solution (20 mL) were added to the mixture to stop the reaction. The resulting mixture was washed by 5% HCl solution to remove metal ions. It was further washed with DI water until the pH value became 7, and it was finally dried under vacuum at 50 °C for 6 h to yield GO.

2.2. Preparation of thiolated graphene (T-graphene)

Graphite oxide (500 mg) and DI water (50 mL) were added to a beaker, and the mixture was sonicated using a tip sonicator (750 Watt Ultrasonic Processor, Sonics) for 20 min at 20% power. Graphite oxide was tip-sonicated to exfoliate the suspension completely and centrifuged at 4000 rpm to remove the unexfoliated graphite oxide. NaSH (8 g) was added gradually with stirring, and the mixture was then ultrasonicated for 1 h at 40 °C. The resulting mixture was kept under stirring for 20 h at 55 °C to produce thiol groups on the surface of graphene oxide. The product was filtered and washed with DI water and dried under vacuum at 50 °C for 3 h. Finally, the dried product was annealed at 150 °C for 3 h in N_2 ambience. Fig. 1a shows the schematic process of T-graphene synthesis.

2.3. Material characterization

The synthesized T-graphene was characterized by various surface, structural and compositional analysis techniques. Graphene hexagonal peaks were identified by high-resolution X-ray diffractometry (HR-XRD, Rigaku) with CuKα radiation (k = 1.540 Å). Raman spectra were obtained with Horiba-Jobin-Yvon equipment using a 514 nm Ar^+ ion laser excitation source with 10 mW power. X-ray photoelectron spectroscopy (MULTILAB 2000 SYSTEM, SSK) was performed for chemical analysis. The surface morphological measurements were carried out by field emission scanning electron microscopy (FESEM S-4700 HITACHI) and high-resolution transmission electron microscopy (HRTEM TECNAI F20 Philips). Fourier transform infrared (FTIR) analysis was also carried out to examine the vibrational characteristics of graphene (IRPrestige-21, Shimadzu). The surface area and porosity of the synthesized powders were determined by the Brunauer–Emmett–Teller (BET) adsorption method and the Barrett-Joyner-Halenda (BJH) method, respectively, using a low-temperature nitrogen-adsorption surface-area analyzer (ASAP 2020, Micromeritics Inc.).

2.4. Electrode fabrication and cell assembly

The working electrode was fabricated with 75 wt% of graphene powder, 18 wt% of Ketjen black and 7 wt% of teflonized acetylene black (TAB) mixed well to slurry, which was pressed on a stainless steel (SS) mesh, under a pressure of 300 kg/cm^2 and dried for 5 h in an oven at 140 °C [39]. Each electrode weighs around 1 mg. The electrochemical measurements were performed using CR2032 cells. A porous polypropylene film (Celgard 3401) was used as a separator. The test cell was fabricated in an argon-filled glove box by pressing together the graphene electrodes separated by the separator. 1-butyl-3-methylimidazolium tetrafluoroborate ($BMIMBF_4$) ionic liquid was used as the electrolyte.

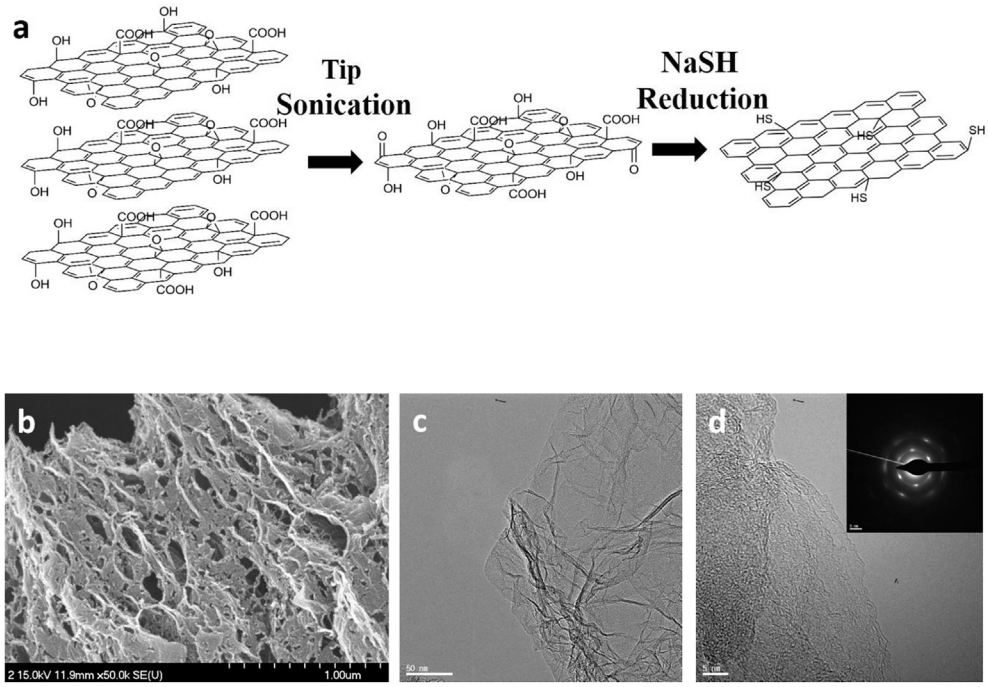

Fig. 1. (a) Schematic process of T-graphene synthesis. (b) SEM micrograph of as-prepared T-graphene. (c and d) HR-TEM images of the T-graphene layers with wrinkles. Inset of (d) shows the corresponding selective area electron diffraction pattern.

2.5. Electrochemical measurements

Cyclic voltammetry (CV) measurements and electrochemical impedance spectroscopy (EIS) analysis were performed using a Zahner electrochemical unit (1M6e, Zahner, Germany). Galvanostatic charge-discharge (C-D) measurements of the symmetric supercapacitor cell were carried out between 0 and 3.5 V at various current densities by using a battery tester (NAGANO, BTS-2004H, Japan). All the electrochemical tests were carried out at room temperature. The specific capacitance C_s (Fg^{-1}) of T-graphene in the symmetric supercapacitor is calculated according to the following formula [15]:

$$C_s = 4I/(mdV/dt),$$

where I is the constant current, m is the total mass of the two electrodes, and dV/dt is the slope of the discharge curve. The specific capacitance is defined as the capacitance of single electrode.

The energy density, E ($Whkg^{-1}$) and the power density, P (Wkg^{-1}) of the symmetric supercapacitors is calculated using the following formulas [15,40]:

$$E = 1/8C_sV^2,$$

$$P = E/\Delta t,$$

where Δt is the discharge time.

3. Results and discussion

3.1. Characterization of synthesized T-graphene

The surface morphology of the T-graphene appears to be highly porous with visible macropores on the surface as shown in the SEM micrograph (Fig. 1b). These macropores, acting as frames, provide a hierarchical network interconnecting with the mesopores, and permit better ion accessibility. High-resolution TEM images of the synthesized T-graphene are shown in Fig. 1c and d. It is clearly seen that the prepared graphene sheets are crippled and wrinkled. Such a structure prevents restacking of the graphene sheets. The resulting graphene nanosheets exhibit an exfoliated structure with a single or a few layers along the edge. The selected area electron diffraction (inset of Fig. 1d) shows a ring-like pattern consisting of six strong diffraction spots corresponding to the hexagonal crystal of graphene.

Nitrogen adsorption isotherm measurement was performed to study the specific surface area and porosity of the T-graphene (Fig. 2a). According to the BET theory, the surface area of T-graphene is estimated to be 437.7 m^2/g. Theoretically-calculated surface area of a single-layer graphene is 2675 m^2/g. The hysteresis between adsorption and desorption along with a sharp fall in the amount of nitrogen adsorbed at higher relative pressures indicates the mesoporous nature of the T-graphene [18]. Note that the BET surface area does not necessarily reflect the actual accessible sites that electrolyte ions can reside inside the pores, when they are packed into an electrode. Thus, the device performance cannot be evaluated by simply taking account of BET surface area. Based on Barret-Joyner-Halenda (BJH) methods, the pore size distribution is within the range of 3.77–4 nm as shown in Fig. 2b. The pore distribution also is extended into the macropore range, in spite of mesopores being the majority. In addition, most of the pores are larger than the diameter of the ionic liquid ions (~0.7 nm), which enables ions to access the pores easily.

The XRD pattern of T-graphene in Fig. 2c shows a broad peak at 24.8°, which corresponds to the (002) hexagonal plane of graphene with an interlayer spacing of 3.76 Å. The XRD data indicates a reduced interlayer spacing of 3.76 Å for T-graphene when it is compared with graphite oxide whose interlayer spacing is 7.1 Å. It implies that most of the oxygen functional groups have been removed during the reduction process [32]. The Raman spectrum of the T-graphene is shown in Fig. 2d. The highly ordered graphite has two Raman peaks: the G band (~1589 cm^{-1}) caused by the in-plane

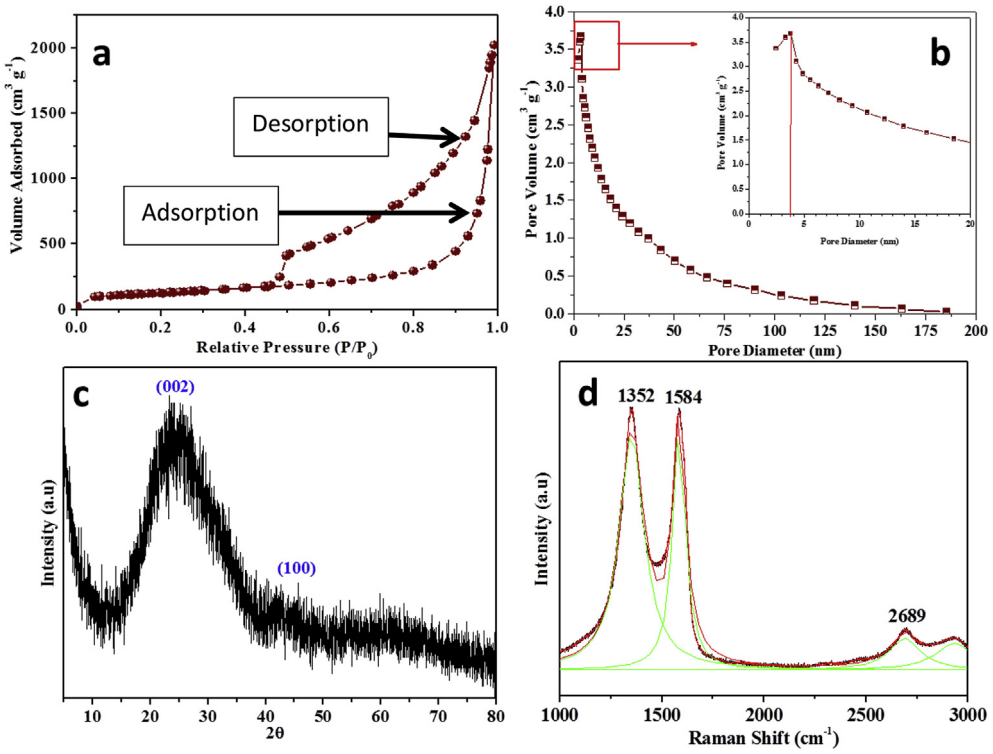

Fig. 2. (a) Nitrogen adsorption and desorption isotherm. (b) Pore-size distribution of T-graphene. (c) X-ray diffraction pattern of graphene powder. (d) Raman spectrum of T-graphene. (A colour version of this figure can be viewed online.)

bond stretching vibration of sp^2-bonded carbon atoms [41] and the weak D band (~1355 cm^{-1}) that resulted from the disorder [42]. In the Raman spectra, two broad peaks were observed at 1350 cm^{-1} and 1584 cm^{-1}. The peak at 1350 cm^{-1} is assigned to the D band, which resulted from the disordered structure [41], and G-band at 1584 cm^{-1} originates from T-graphene. The G-band is redshifted from the undoped graphene peak at 1589 cm^{-1}. The red shift can be ascribed to the insertion of the thiol group on the graphene layer [37]. Moreover, the 2D peak at 2689 cm^{-1} confirms the presence of single- or few-layered graphene sheets.

The XPS spectrum of the T-graphene in Fig. 3a shows that the sharp C1s peak at 284.6 eV, which is attributed to sp^2 carbon. The full-width at half-maximum (FWHM) of the main sp^2 carbon peak of the T-graphene is 1.18 eV, which is close to the highly oriented pyrolytic graphite [43]. The other peaks at 286, 287, and 291 eV are assigned to the hydroxyl group (C-OH) group, carbonyl group (C=O), and carboxyl group (COOH), respectively [33,44]. The total atomic ratio of C/O in the T-graphene from quantitative analysis is 28. The C/O ratio is higher than the previously reported value of graphene reduced by hydrazine [26,33], $NaBH_4$ [35], and urea [45]. This confirms the excellent reduction of GO by NaSH as a reducing agent. The weaker oxide peaks compared with C1s peak indicate that the amount of residual functional groups is very low compared to the C1s peak. The S2p core level spectrum of T-graphene in Fig. 3b shows a asymmetric peak at 163.3eV that is assigned to the thiolate bond of C-S-H [37,46,47].

The FT-IR spectrum of the T-graphene (Fig. 3c) shows strong peaks at 3433 cm^{-1} and 1629 cm^{-1} which are assigned to stretching and bending vibrations of the OH groups in water molecules absorbed on the T-graphene [48]. The bands at 2925 and 2853 cm^{-1} correspond to the C-H stretch vibrations of the methylene group and the peak observed at 1195 cm^{-1} corresponds to C-OH stretching vibration in COOH groups. The weak peak intensities of those oxygen containing groups indicate that a considerable number of the them are removed. Notably, two peaks at 671 cm^{-1} and 800 cm^{-1} are observed, which are associated with C-S stretching and C-SH bending [49]. This indicates that a fraction of OH groups in graphene oxide has been exchanged to SH groups in T-graphene.

3.2. Electrochemical performance of symmetric T-graphene supercapacitors

To measure the electrochemical performance of the T-graphene, supercapacitor cells with symmetrical geometry were prepared using ionic liquid $BMIMBF_4$ as an electrolyte. The CV curves of T-graphene electrodes obtained at scan rates from 5 to 30 mVs^{-1} are shown in Fig. 4a. The device exhibited increased current response with the increase in scan rate, indicating a capacitive behavior. No redox peaks in the rectangular shape CV curves were observed for all scan rates, implying that the electrode material exhibits an electrical double-layer capacitor behavior without any pseudo-capacitance effect due to functional groups.

The charging and discharging properties of the T-graphene were measured between 0 and 3.5 V at various current densities ranging from 2.5 to 7.5 Ag^{-1}, and the corresponding C-D curves are presented in Fig. 4b. The typical triangular shaped C-D curves demonstrate the double-layer capacitance behavior of the electrodes with no Faradic redox reaction due to the fact that the oxygen functional groups are effectively removed. The C-D curves are almost symmetric because the electrochemical adsorption and desorption takes place at the electrode-electrolyte interface. It is also noted that the charging and discharging times of the supercapacitor were almost the same, suggesting a high Coulombic efficiency. The calculated Coulombic efficiency is as high as 98%. The C-D curves show a small voltage drop arising from the equivalent series resistance.

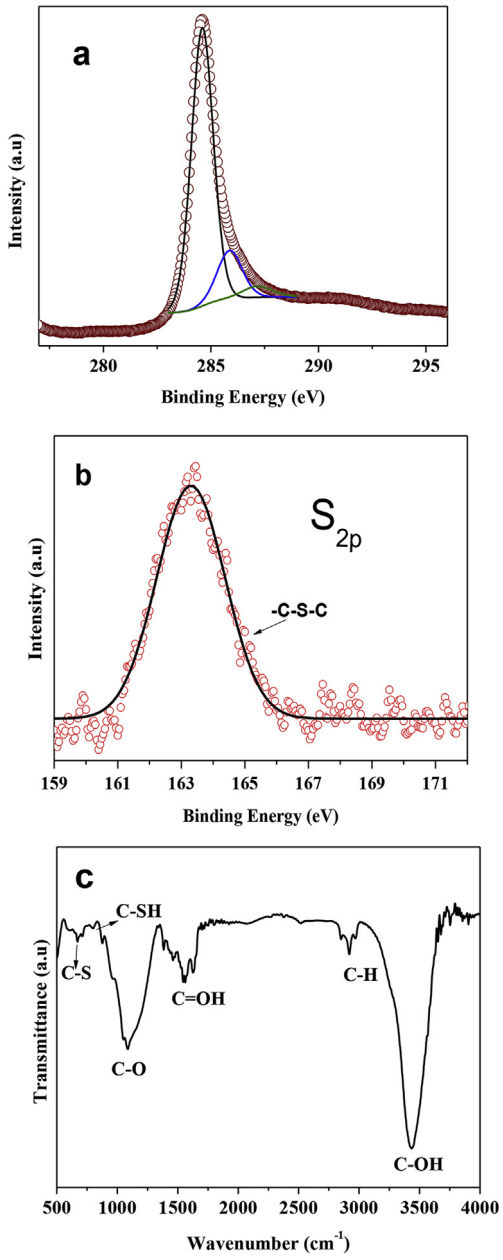

Fig. 3. (a) XPS C1s spectrum of T-graphene. (b) S2p core-level spectrum for T-graphene (c) FTIR spectrum of as prepared T-graphene. (A colour version of this figure can be viewed online.)

The electrochemical performance of a material can be evaluated by the specific capacitance, C_s [15]. As the charging current density increases, the specific capacitance value decreases from 196 Fg^{-1} to 137 Fg^{-1}, as shown in Table 1. At these current densities, the measured power density values are 4.3, 9.2, 13.1 $kWkg^{-1}$, respectively. The high specific capacitance can be ascribed to the greater porosity and conjugation structure of the T-graphene which improves fast ion movements during the charging-discharging process. It is obvious that the capacitance decreases when increasing current density. This is due to the low penetration possibility of ions into the inner region of pores and also the rapid potential changes. The supercapacitors in this study exhibited high specific capacitance compared with other reported values at similar current density, shown in Table 2.

Since long-term cycling of supercapacitors at high current is an essential for high-power applications, the stability of the T-graphene electrodes was evaluated at a constant current density of 7.5 Ag^{-1} for 10,000 cycles. As shown in Fig. 4c, the specific capacitance difference between the 1st and 10,000th cycle is very small, demonstrating its excellent electrochemical stability. The specific capacitance initially dropped by 2% during the first 400 cycles and then remained almost constant until 10,000 cycles.

The electrochemical impedance spectra for the T-graphene electrodes are shown in Fig. 4d. The Nyquist plot of the T-graphene-based supercapacitor shows an inclined line in the low-frequency region and a semicircle in the high-frequency region. The straight line at low frequency indicates a nearly ideal capacitor response [33]. The equivalent series resistance (ESR) value obtained from the x-intercept of the Nyquist plot is 4.2 Ω. The ESR value increases to 6.4 Ω after 10,000 cycles. The increased ESR value may be relevant to the slight expansion of electrode after repeated cycling.

The energy density as a function of current density is shown in Table 1. The energy density values are 83.4, 64.2, and 58.3 $Whkg^{-1}$ at current density values of 2.5, 5, and 7.5 Ag^{-1}, respectively. And, the corresponding discharging time are 69, 25, and 16 s, respectively. The graphene-based supercapacitor reported by Liu et al. is capable of storing 67.7 $Whkg^{-1}$, which is equivalent to the energy capacity of a Ni metal hydride battery [18]. It is noteworthy that the T-graphene based supercapacitor in this study exhibits a similar energy capacity of 64.2 $Whkg^{-1}$, and it can be charged within 25 s. The T-graphene supercapacitor can be charged almost two times faster than the device reported by Liu et al. [18]. The energy density values of the T-graphene are superior to those of the graphene-based supercapacitors reported in the literature recently [50–63]. The Columbic efficiency is calculated as the ratio between the released charge during discharging and the stored charge during charging. The Columbic efficiencies of our graphene supercapacitors are 99.4%, 99.2% and 97.5% at 2.5 A/g, 5 A/g and 7.5 A/g. The round-trip efficiency is defined as the ration between energy released during discharging and the total input energy during charging. The round-trip efficiencies of the T-graphene supercapacitors are 71.2%, 65.0% and 58.2% at 2.5 A/g, 5 A/g and 7.5 A/g.

The superior specific capacitance and energy density of the T-graphene based supercapacitor could be attributed to the compression method used to prepare electrodes and high ion accessibility on the surface. The power and energy density obtained at the high current density of 7.5 Ag^{-1} are 13.1 $kWkg^{-1}$ and 58.3 $Whkg^{-1}$, respectively. The superior performance of the supercapacitor may allow it to find applications in heavy duty equipment [33,34]. To the best of our knowledge, this is the first report on the utilization of T-graphene in supercapacitors.

4. Conclusion

A simple route to prepare T-graphene using NaSH as a reducing agent is reported. It was found that NaSH is highly effective in removing most of the oxygen containing groups from graphite oxide. The C/O ratio is as high as 28 after reduction. When using the synthesized T-graphene as electrodes, the supercapacitor exhibited a specific capacitance of 196 Fg^{-1}, a power density of 4.3 $kWkg^{-1}$, and an energy density of 83.4 $Whkg^{-1}$ at a current density of 2.5 Ag^{-1}. Even at high current density of 7.5 Ag^{-1}, 98% of the starting capacitance was retained after 10,000 cycles. The porous structure of the highly reduced nature of T-graphene enhanced the ion accessibility. The T-graphene based supercapacitor with high electrochemical performance and stability at high current density is suitable for high-power applications.

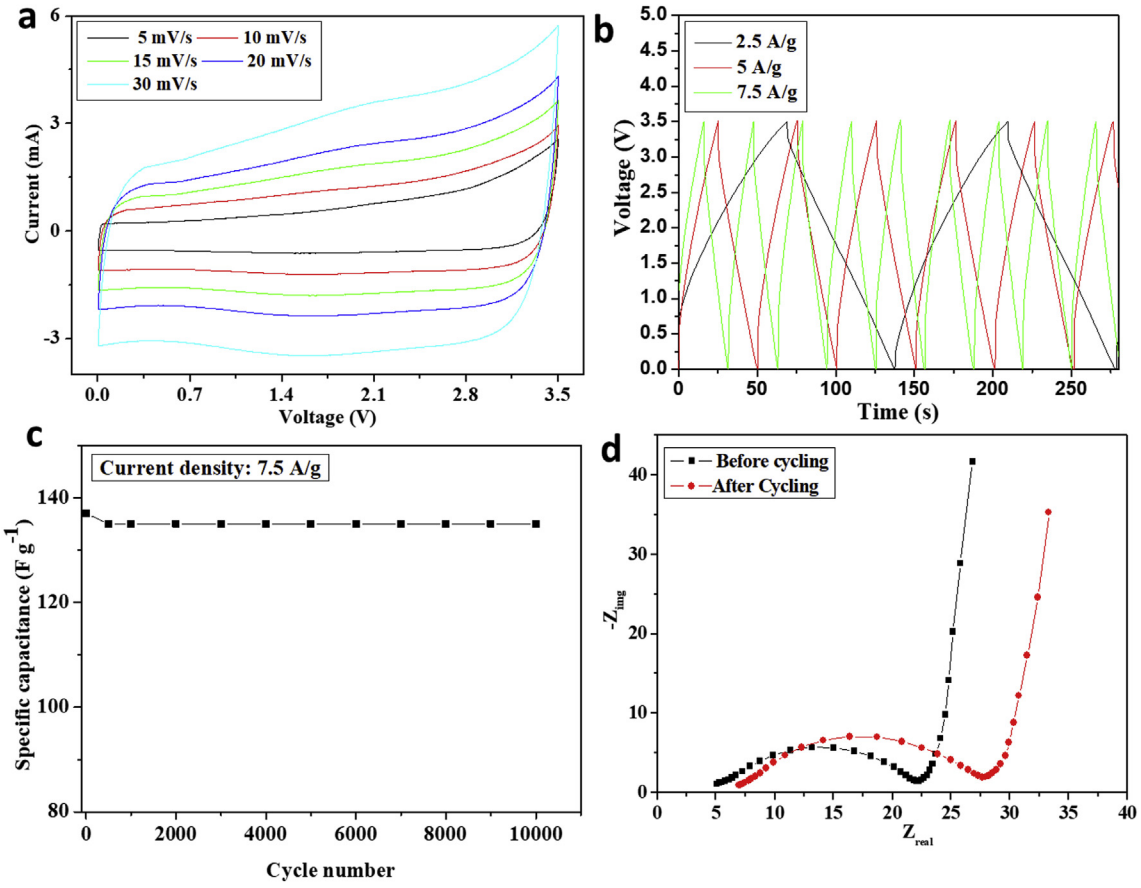

Fig. 4. (a) C-V curves of T-graphene based supercapacitor. (b) Charge-discharge curve of the T-graphene based supercapacitor at various current densities of 2.5 Ag^{-1}, 5 Ag^{-1}, 7.5 Ag^{-1}. (c) Cycle performance of T-graphene based supercapacitor at a current density of 7.5 Ag^{-1}. (d) Electrochemical impedance spectra of T-graphene based supercapacitor. (A colour version of this figure can be viewed online.)

Table 1
The specific capacitance, energy density, and power density of the graphene supercapacitor at different current densities.

Current density (A/g)	Specific capacitance (F/g)	Energy density (Wh/kg)	Power density (W/kg)
2.5	196	83.4	4375
5	150	61.3	8750
7.5	137	58.3	13,125

Table 2
Performance comparison of graphene-based supercapacitors.

Material	Electrolyte	Current density (A/g)	Specific capacitance (F/g)	Reference
a-MEGO	$BMIMBF_4$/AN	2.8	166	[15]
Curved graphene	$EMIMBF_4$	2	137	[18]
VAG	$EMIMBF_4$	2	206	[32]
HAG	$EMIMBF_4$	2	259	[50]
ARAG	$EMIMBF_4$	2	193	[51]
NRG	KOH	2	~175	[52]
LC GO-PP	H_2SO_4	2	77	[53]
RGO	$LiPF_6$	2	~75	[54]
T-graphene	$BMIMBF_4$	2.5	196	Our work

Acknowledgement

This work was supported by the National Research Foundation of Korea through the World Class University (WCU) program at GIST (Grant No.20110017603).

References

[1] J.R. Miller, P. Simon, Materials science. Electrochemical capacitors for energy management, Science 321 (2008) 651–652.
[2] B.E. Conway, Transition from "supercapacitor" to "battery" behavior in electrochemical energy storage, J. Electrochem. Soc. 138 (1991) 1539–1548.

[3] P. Simon, Y. Gogotsi, Materials for electrochemical capacitors, Nat. Mater. 7 (2008) 845–854.
[4] A. Burke, Ultracapacitors: why, how, and where is the technology, J. Power Sources 91 (2000) 37–50.
[5] A. Burke, R&D considerations for the performance and application of electrochemical capacitors, Electrochim. Acta 53 (2007) 1083–1091.
[6] P.V.D. Bossche, F. Vergels, J.V. Mierlo, J. Matheys, W.V. Autenboer, SUBAT: an assessment of sustainable battery technology, J. Power Sources 162 (2006) 913–919.
[7] J. Baker, New technology and possible advances in energy storage, Energy Pol. 36 (2008) 4368–4373.
[8] M. Conte, P.P. Prosini, S. Passerini, Overview of energy/hydrogen storage: state-of-the-art of the technologies and prospects for nanomaterials, Mater. Sci. Eng. B 108 (2004) 2–8.
[9] L. Damen, J. Hassoun, M. Mastragostino, B. Scrosati, Solid-state, rechargeable Li/LiFePO4 polymer battery for electric vehicle application, J. Power Sources 195 (2010) 6902–6904.
[10] M.E. Roberts, D.R. Wheeler, B.B. McKenzie, B.C. Bunker, High specific capacitance conducting polymer supercapacitor electrodes based on poly(-tris(thiophenylphenyl)amine), J. Mater. Chem. 19 (2009) 6977–6979.
[11] A. Izadi-Najafabadi, S. Yasuda, K. Kobashi, T. Yamada, D.N. Futaba, H. Hatori, M. Yumura, S. Iijima, K. Hata, Extracting the full potential of single-walled carbon nanotubes as durable supercapacitor electrodes operable at 4 V with high power and energy density, Adv. Mater. 22 (2010) E235.
[12] H. Lin, L. Li, J. Ren, Z. Cai, L. Qiu, Z. Yang, H. Peng, Conducting polymer composite film incorporated with aligned carbon nanotubes for transparent, flexible and efficient supercapacitor, Sci. Rep. 3 (2013) 1353.
[13] M.D. Stoller, S. Park, Y. Zhu, J. An, R.S. Ruoff, Graphene-based ultracapacitors, Nano Lett. 8 (2008) 3498–3502.
[14] B. Xu, S.F. Yue, Z.Y. Sui, X.T. Zhang, S.S. Hou, G.P. Cao, Y.S. Yang, What is the choice for supercapacitors: graphene or graphene oxide, Energy Environ. Sci. 4 (2011) 2826–2830.
[15] S. Murali, M.D. Stoller, K.J. Ganesh, W. Cai, P.J. Ferreira, A. Pirkle, R.M. Wallace, K.A. Cychosz, M. Thommes, D. Su, E.A. Stach, R.S. Ruoff, Carbon-based supercapacitors produced by activation of graphene, Science 332 (2011) 1537–1541.
[16] Q. Wu, Y.X. Xu, Z.Y. Yao, A.R. Liu, G.Q. Shi, Supercapacitors based on flexible graphene/polyaniline nanofiber composite films, ACS Nano 4 (2010) 1963–1970.
[17] Q. Hao, H. Wang, X. Yang, L. Lu, X. Wang, Morphology-controlled fabrication of sulfonated graphene/polyaniline nanocomposites by liquid/liquid interfacial polymerization and investigation of their electrochemical properties, Nano Res. 4 (2011) 323–333.
[18] C. Liu, Z. Yu, D. Neff, A. Zhamu, B.Z. Jang, Graphene-based supercapacitor with an ultrahigh energy density, Nano Lett. 10 (2010) 4863–4868.
[19] K. Karthikeyan, S. Amaresh, V. Aravindan, Y.S. Lee, Microwave assisted green synthesis of MgO–carbon nanotube composites as electrode material for high power and energy density supercapacitors, J. Mater. Chem. A. 1 (2013) 4105–4111.
[20] K. Karthikeyan, D. Kalpana, S. Amaresh, Y.S. Lee, Microwave synthesis of graphene/magnetite composite electrode material for symmetric supercapacitor with superior rate performance, RSC Adv. 2 (2012) 12322–12328.
[21] Z.P. Li, J.Q. Wang, X.H. Liu, S. Liu, J.F. Ou, S.R. Yang, Electrostatic layer-by-layer self-assembly multilayer films based on graphene and manganese dioxide sheets as novel electrode materials for supercapacitors, J. Mater. Chem. 21 (2011) 3397–3403.
[22] J.Y. Zhu, J.H. He, Facile synthesis of graphene-wrapped honeycomb MnO2 nanospheres and their application in supercapacitors, ACS Appl. Mater. Interfaces 4 (2012) 1770–1776.
[23] J.W. Xiao, S.H. Yang, Bio-inspired synthesis of NaCl-type CoxNi1−xO ($0 \leq x < 1$) nanorods on reduced graphene oxide sheets and screening for asymmetric electrochemical capacitors, J. Mater. Chem. 22 (2012) 12253–12262.
[24] S. Park, R.S. Ruoff, Chemical methods for the production of graphenes, Nat. Nanotechnol. 4 (2009) 217–224.
[25] W.S. Hummers Jr., R.E. Offeman, Preparation of graphitic oxide, J. Am. Chem. Soc. 80 (1958), 1339–1339.
[26] S. Stankovich, D.A. Dikin, R.D. Piner, K.A. Kohlhaas, A. Kleinhammes, Y. Jia, Y. Wu, S.T. Nguyen, R.S. Ruoff, Synthesis of graphene-based nanosheets via chemical reduction of exfoliated graphite oxide, Carbon 45 (2007) 1558–1565.
[27] H.C. Schniepp, J.L. Li, M.J. McAllister, H. Sai, M.H. Alonso, D.H. Adamson, R.K. Pruddhomme, R. Car, D.A. Saville, I.A. Aksay, Functionalized single graphene sheets derived from splitting graphite oxide, J. Phys. Chem. B 110 (2006) 8535–8539.
[28] S. Park, J.H. An, R.D. Piner, I. Jung, D.X. Yang, A. Velamakanni, S.T. Nguyen, R.S. Ruoff, Aqueous suspension and characterization of chemically modified graphene sheets, Chem. Mater. 20 (2008) 6592–6594.
[29] U. Khan, A.O. Neill, M. Lotya, S. De, J.N. Coleman, High-concentration solvent exfoliation of graphene, Small 6 (2010) 864–871.
[30] Y. Zhu, M. Shanthi, M.D. Stoller, V. Aruna, R.D. Piner, R.S. Ruoff, Microwave assisted exfoliation and reduction of graphite oxide for ultracapacitors, Carbon 48 (2010) 2106–2122.
[31] C.T.J. Low, F.C. Walsh, M.H. Chakrabarti, M.A. Hashim, M.A. Hussain, Electrochemical approaches to the production of graphene flakes and their potential applications, Carbon 54 (2013) 1–21.
[32] H. Yang, S. Kannappan, A. Samuthirapandian, J.H. Jang, Y.S. Lee, W. Lu, Nanoporous graphene materials by low-temperature vacuum-assisted thermal process for electrochemical energy storage, J. Power Sources 284 (2015) 146–153.
[33] D. Li, M.B. Muller, S. Gilje, R.B. Kaner, G.G. Wallace, Processable aqueous dispersions of graphene nanosheets, Nat. Nanotechnol. 3 (2008) 101–105.
[34] X. Fan, W. Peng, Y. Li, X. Li, S. Wang, G. Zhang, F. Zhang, Deoxygenation of exfoliated graphite oxide under alkaline conditions: a Green route to graphene preparation, Adv. Mater. 20 (2008) 4490–4493, 2008.
[35] W. Gao, L.B. Alemany, L. Ci, P.M. Ajayan, New insights into the structure and reduction of graphite oxide, Nat. Chem. 1 (2009) 403–408.
[36] G. Wang, J. Yang, J. Park, X. Gou, B. Wang, H. Liu, J. Yao, Facile synthesis and characterization of graphene nanosheets, J. Phys. Chem. C 112 (2008) 8192–8195.
[37] J.D. Kim, T. Palani, M. Rajesh Kumar, S. Lee, H.C. Choi, Preparation of reusable Ag-decorated graphene oxide catalysts for decarboxylative cycloaddition, J. Mater. Chem. 22 (2012) 20665–20670.
[38] N.I. Kovtyukhova, P.J. Ollivier, B.R. Martin, T.E. Mallouk, S.A. Chizhik, E.V. Buzaneva, A.D. Gorchinskiy, Layer-by-Layer assembly of ultrathin composite films from micron-sized graphite oxide sheets and polycations, Chem. Mater. 11 (1999) 771–778, 1999.
[39] K. Karthikeyan, S. Amaresh, K.J. Kim, S.H. Kim, K.Y. Chung, B.W. Cho, Y.S. Lee, A high performance hybrid capacitor with Li2CoPO4F cathode and activated carbon anode, Nanoscale 5 (2013) 5958–5964, 2013.
[40] M.F. El-Kady, V. Strong, S. Dubin, R.B. Kaner, Laser scribing of high-performance and flexible graphene-based electrochemical capacitors, Science 335 (2012) 1326–1330.
[41] Y. Liu, R. Deng, Z. Wang, H. Liu, Carboxyl-functionalized graphene oxide–polyaniline composite as a promising supercapacitor material, J. Mater. Chem. 22 (2012) 13619–13624.
[42] A.C. Ferrari, J. Robertson, Interpretation of Raman spectra of disordered and amorphous carbon, Phys. Rev. B 61 (2000), 14095.
[43] J.A. Leiro, M.H. Heinonen, T. Laiho, I.G. Batirev, Core-level XPS spectra of fullerene, highly oriented pyrolitic graphite, and glassy carbon, J. Electron. Spectrosc. Relat. Phenom. 128 (2003) 205–213.
[44] S. Stankovich, R.D. Piner, X.Q. Chen, N.Q. Wu, S.T. Nguyen, R.S. Ruoff, Stable aqueous dispersions of graphitic nanoplatelets via the reduction of exfoliated graphite oxide in the presence of poly(sodium 4-styrenesulfonate), J. Mater. Chem. 16 (2006) 155–158.
[45] Z. Lei, L. Lu, X.S. Zhao, The electrocapacitive properties of graphene oxide reduced by urea, Energy Environ. Sci. 5 (2013) 6391–6399.
[46] C. Médard, M. Morin, Chemisorption of aromatic thiols onto a glassy carbon surface, J. Electroanal. Chem. 632 (2009) 120–126.
[47] L.G. Bach, Md R. Islam, J.T. Kim, S. Seo, K.T. Lim, Encapsulation of Fe3O4 magnetic nanoparticles with poly(methyl methacrylate) via surface functionalized thiol-lactam initiated radical polymerization, Appl. Surf. Sci. 258 (2012) 2959–2966.
[48] A. Bagri, C. Mattevi, M. Acik, Y.J. Chabal, M. Chhowalla, V.B. Shenoy, Structural evolution during the reduction of chemically derived graphene oxide, Nat. Chem. 2 (2010) 581.
[49] C.V. Pham, M. Eck, M. Krueger, Thiol functionalized reduced graphene oxide as a base material for novel graphene-nanoparticle hybrid composites, Chem. Eng. J. 231 (2013) 146–154.
[50] H. Yang, S. Kannappan, A. Samuthirapandian, J.H. Jang, Y.S. Lee, W. Lu, Graphene supercapacitor with both high power and energy density, Nanotechnology 28 (2017), 445401.
[51] H. Yang, S. Kannappan, A. Samuthirapandian, J.H. Jang, Y.S. Lee, W. Lu, Rapidly annealed nanoporous graphene materials for electrochemical energy storage, J. Mater. Chem. 5 (2017) 23720–23726.
[52] L. Li, H. Bi, S. Gai, F. He, P. Gao, Y. Dai, X. Zhang, D. Yang, M. Zhang, P. Yang, Uniformly dispersed ZnFe2O4 nanoparticles on nitrogen-modified graphene for high-performance supercapacitor as electrode, Sci. Rep. 7 (2017), 43116.
[53] M.M. Islam, A.T. Chidembo, S.H. Aboutalebi, D. Cardillo, H.K. Liu, K. Konstantinov, S.X. Dou, Liquid crystalline graphene oxide/PEDOT: PSS self-assembled 3D architecture for binder-free supercapacitor electrodes, Front. Energy Res. 2 (2014) 31.
[54] S. Shivakumaraz, B. Kishore, T.R. Penki, N. Munichandraiah, Symmetric supercapacitor based on reduced graphene oxide in non-aqueous electrolyte, ECS Electrochem. Lett. 4 (2015) A87–A89.
[55] T.Y. Kim, G. Jung, S. Yoo, K.S. Suh, R.S. Ruoff, Activated graphene-based carbons as supercapacitor electrodes with macro- and mesopores, ACS Nano 7 (2013) 6899–6905.
[56] J. Han, L.L. Zhang, S. Lee, J. Oh, K.S. Lee, J.R. Potts, J. Ji, X. Zhao, R.S. Ruoff, S. Park, Generation of B-Doped graphene nanoplatelets using a solution process and their supercapacitor applications, ACS Nano 7 (2013) 19–26.
[57] B. You, J. Jiang, S. Fan, Three-dimensional hierarchically porous all-carbon foams for supercapacitor, ACS Appl. Mater. Interfaces 6 (2014) 15302–15308.
[58] J.H. Lee, N. Park, B.G. Kim, D.S. Jung, K. Im, J. Hur, J.W. Choi, Restacking-inhibited 3D reduced graphene oxide for high performance supercapacitor electrodes, ACS Nano 7 (2013) 9366–9374.
[59] J.J. Yoo, K. Balakrishnan, J. Huang, V. Meunier, B.G. Sumpter, A. Srivastava, M. Conway, A.M. Reddy, J. Yu, R. Vajtai, P.M. Ajayan, Ultrathin planar graphene supercapacitors, Nano Lett. 11 (2011) 1423–1427.
[60] Y. Wang, Z. Shi, Y. Huang, Y. Ma, C. Wang, M. Chen, Y. Chen, Supercapacitor devices based on graphene materials, J. Phys. Chem. C 113 (2009)

13103–13107.
[61] N. Xiao, H. Tan, J. Zhu, L. Tan, X. Rui, X. Dong, Q. Yan, High-performance supercapacitor electrodes based on graphene achieved by thermal treatment with the aid of nitric acid, ACS Appl. Mater. Interfaces 5 (2013) 9656–9662.
[62] Z. Xu, Z. Li, C.M.B. Holt, X. Tan, H.W.S. Amirkhiz, T. Stephenson, D. Mitlin, Electrochemical supercapacitor electrodes from sponge-like graphene nanoarchitectures with ultrahigh power density, J. Phys. Chem. Lett. 3 (2012) 2928–2933.
[63] L. Lai, H. Yang, L. Wang, B.K. Teh, J. Zhong, H. Chou, L. Chen, W. Chen, Z. Shen, R.S. Ruoff, J. Lin, Preparation of supercapacitor electrodes through selection of graphene surface functionalities, ACS Nano 7 (2013) 5941–5951.